Zero-Age Main Sequence Stellar Structure

PHYS 6260 Project Proposal

Brandon Pries

School of Physics, Georgia Institute of Technology,
Atlanta, GA 30318

May 1, 2023

Abstract

Stellar structure is a complex topic that lies at the intersection of several fields of physics: quantum mechanics, statistical mechanics, thermodynamics, hydrodynamics, radiative transport, nuclear processes, particle physics, and electromagnetism, to name a few. Stellar structure is a multi-dimensional problem that requires rigorous modeling to produce results that agree with observations. Here, I attempt to implement a computational model of stellar structure, accounting for a variety of interior processes in the star; in particular, I will attempt to model the zero-age main sequence (ZAMS), which is the ignition point of hydrogen fusion in the core of the star. The results produced from this study are unconverged, but the model is able to accurately recover certain behaviors and effects. These results demonstrate the complexity and computational cost of modeling stellar evolution, even in simplified cases like ZAMS and time-independent integration.

1 Introduction

1.1 Overview

Stellar structure has been studied in detail for nearly two centuries. Though many individual pieces are well-understood, modeling the interplay between these various components can be challenging. This is a problem that must be solved numerically; the scaling of this problem is simply infeasible to replicate in laboratory environments, though experiments can isolate individual processes (e.g., nuclear reactions, particle physics, plasmas, etc.). We also have a plethora of observational data that we can compare to, but the models of stellar structure themselves must be computational.

1.2 Literature Review

Much of the work in the theory of stellar structure has been developed since the formulation of the law of conservation of energy in the mid-19$^{\text{th}}$ century [1]. If the Sun were radiating energy to Earth, it must be getting energy from somewhere. Early theories suggested meteor bombardment, chemical burning, and gravitational contraction, but the lifetimes predicted by these processes were wildly contradictory to geologic estimates for the age of the Earth [1]. It was not until the 1930's when Hans Bethe's work in nuclear processes led to him to suggest a thermonuclear source of energy (namely, the CNO cycle, for which he won the Nobel Prize in Physics in 1967) [2, 3].

The equation(s) of state are typically derived from a combination of quantum mechanics, statistical mechanics, thermodynamics, and nuclear physics principles; additional considerations often come from fields like hydrodynamics, transport processes, and particle physics. The equations of stellar structure come from assumptions like local thermodynamic equilibrium (LTE), continuity, energy transport, and conservation of mass-energy [4]. These will be discussed in further detail in later sections.

In modern times, the equations of stellar structure are solved numerically using large code suites like MESA [5]. These suites can also account for stellar evolution (i.e., explicit time dependence) for processes like chemical evolution, radial oscillations, mass loss, and stellar winds.

As previously alluded to, this model means little without the real-world data that validates its performance, and I would be remiss to neglect a discussion of its history. Many observers gathered spectra of stars in the early 20$^{\text{th}}$ century to get a better understanding of stellar characteristics. Following Planck's developments in radiative processes like blackbody radiation [6], astronomers could estimate stars' surface temperatures from these spectra; combined with distance estimates from parallax measurements, scientists could then calculate the stars' total luminosities. Hertzsprung and Russel independently discovered a

relationship between the surface temperatures and luminosities of stars [7–9], finding that many of them lie along a narrow strip when plotted in luminosity-temperature (L-T) phase space. This strip represents the main sequence, and plots of stars in this phase space are now called Hertzsprung-Russel (HR) diagrams in their honor. Shortly thereafter, Annie Jump Cannon developed a classification scheme for stars based on the strength of their Balmer absorption lines and showed that this was analagous to classifying them using surface temperature [10, 11].

In recent years, much of the data collection and cataloguing is done by telescopes. This includes *Hipparcos* [12–14], a European Space Agency (ESA) mission intended to catalogue astrometric data for $\mathcal{O}(10^5)$ stars in the neighborhood of the Sun; and *Gaia* [15–17], an ESA mission and *Hipparcos*' successor, that will be taking a census of $\mathcal{O}(10^9)$ stars in the Milky Way. *Gaia* data has led to the development of the most robust HR diagrams in history [17].

1.3 Project Scope

In this project, I will attempt to create a numerical suite that can model the time-independent equations of stellar structure and produce continuous profiles of variables throughout the star. I will be focusing on ZAMS stars, using the test case of the Sun since this is the most well-studied star and has the best observational data to compare to. In principle, each star is uniquely defined by its total mass and chemical composition, which could vary throughout the star; however, under the ZAMS scenario, I will assume that the chemical composition is isotropic throughout the star. Again, since this is time-independent, I will neglect effects like chemical evolution and transport.

The structure for the remainder of the report is as follows: in Section 2, I will discuss in detail the underlying physics that requires modeling; in Section 3, I will describe the numerical implementation of the model; in Section 4, I will present the available results and their achievements/shortcomings; and in Section 5, I will conclude and discuss potential pathways for improvement.

2 Physics of Stellar Structure

2.1 Variables

Before considering the physical equations, I will preface the important variables and constants used in the work shown here. My model considers stars as concentric mass shells, so the independent variable is the mass coordinate m. The four primary variables that define the structure of the star are the radius r, pressure P, luminosity L, and temperature T. Other variables given by the equations of state include the density ρ, reduced luminosity ϵ,

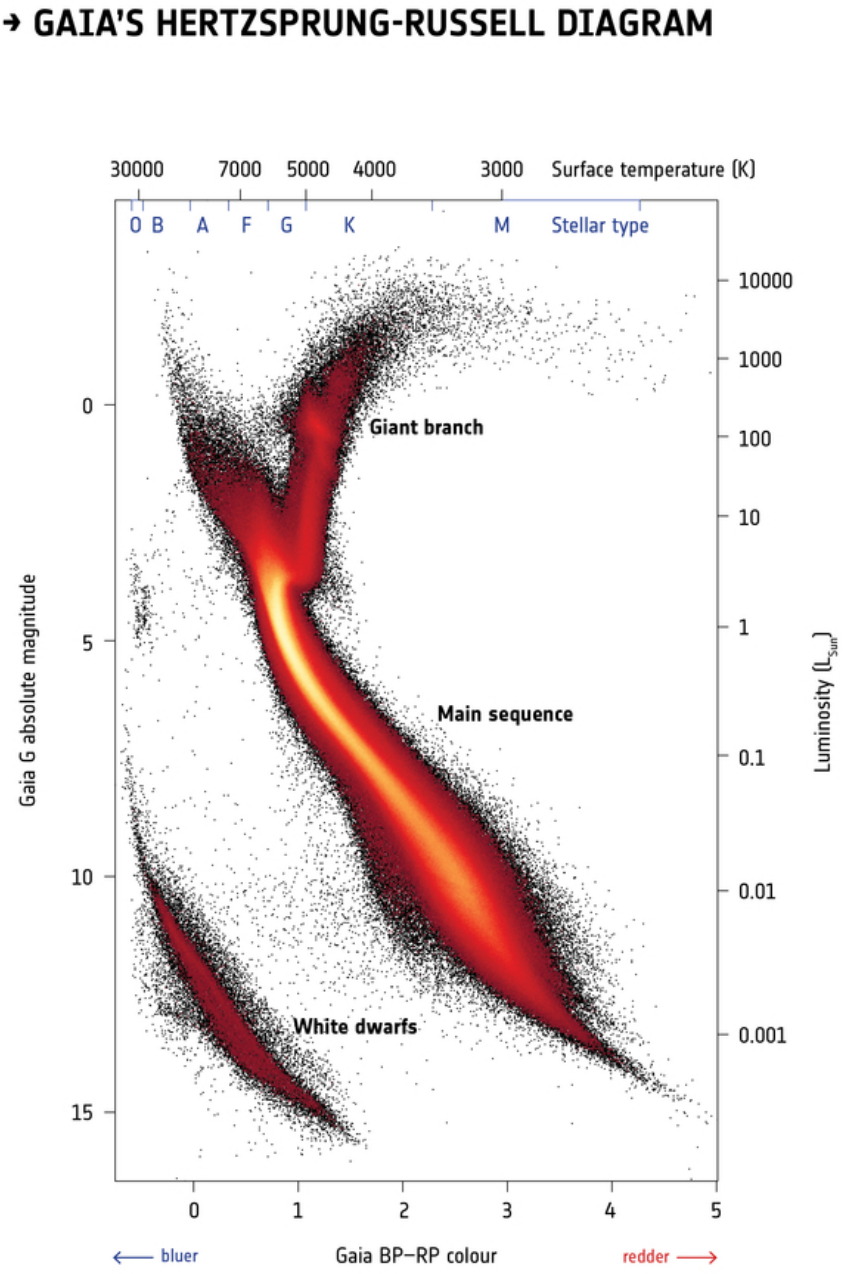

Figure 1: HR diagram of approximately 4.5 million stars from *Gaia* Data Release 2 [17].

and opacity κ. The chemical composition $\vec{X}$ is an array of mass fractions for different species (e.g., H, He, Li, ...).

Symbol	Meaning	Units (SI)
M	Total mass	kg
X_i	Species mass fraction	–
m	Mass coordinate	kg
r	Radius	kg
P	Pressure	Pa
L	Luminosity	W
T	Temperature	K
ρ	Density	$\mathrm{kg/m^3}$
ϵ	Reduced luminosity	W/kg
κ	Opacity	$\mathrm{m^2/kg}$
μ	Mean molecular weight	Atomic Mass Units (AMU)

Table 1: Variables used in project.

These variables are accompanied by a variety of astrophysical constants, detailed in Table 2 in the appendix. These include constants like the atomic numbers and masses of different species; particle masses; quantum mechanical, thermodynamic, and electromagnetic constants; and constants for the Sun used in stellar scalings. The atomic numbers and masses of different species are listed in Table 3, also in the appendix.

2.2 Equations of State

First, I will define the mean molecular weights for ions μ_{ions} and electrons μ_e [4], as these variables are used in many other equations of state.

$$\frac{1}{\mu_{\text{ions}}\left(\vec{X}\right)} = \sum_i \frac{X_i}{\mathcal{A}_i} \tag{1a}$$

$$\frac{1}{\mu_e\left(\vec{X}\right)} = \sum_i \frac{X_i \mathcal{Z}_i}{\mathcal{A}_i} \tag{1b}$$

The primary equation of state describes the relationship between the pressure P, the density ρ, and the temperature T:

$$P\left(\vec{X}, \rho, T\right) = P_{\text{ions}}\left(\vec{X}, \rho, T\right) + P_e\left(\vec{X}, \rho, T\right) + P_{\text{rad}}(T) \tag{2}$$

$$P_{\text{ions}}\left(\vec{X},\rho,T\right) = \frac{\rho}{\mu_{\text{ions}}\left(\vec{X}\right)}k_B T \tag{3a}$$

$$P_e\left(\vec{X},\rho,T\right) = \begin{cases} \frac{\rho}{\mu_e\left(\vec{X}\right)m_u}k_B T & \text{non-degenerate, non-relativistic} \\ \frac{h^2}{20m_e}\left(\frac{3}{\pi}\right)^{2/3}\left(\frac{\rho}{\mu_e\left(\vec{X}\right)m_u}\right)^{5/3} & \text{degenerate, non-relativistic} \\ \frac{hc}{8}\left(\frac{3}{\pi}\right)^{1/3}\left(\frac{\rho}{\mu_e\left(\vec{X}\right)m_u}\right)^{4/3} & \text{degenerate, relativistic} \end{cases} \tag{3b}$$

$$P_{\text{rad}}(T) = \frac{4}{3}\frac{\sigma_{SB}}{c}T^4 \tag{3c}$$

Note that Equation (3b) is a piecewise function that depends on whether or not the electrons are degenerate and/or relativistic. There exist critical densities at the transition points ($\rho_{\text{trans,d}}$ and $\rho_{\text{trans,r}}$, respectively) which come from equating the expressions for P_e on either side of the transition point. This leads us to

$$\rho_{\text{trans,d}}\left(\vec{X},T\right) = \left(\frac{20m_e k_B}{h^2}\right)^{3/2}\frac{\pi m_u}{3}\mu_e\left(\vec{X}\right)T^{3/2} \tag{4a}$$

$$\rho_{\text{trans,r}}\left(\vec{X}\right) = \left(\frac{5}{2}\frac{m_e c}{h}\right)^{3}\frac{\pi m_u}{3}\mu_e\left(\vec{X}\right) \tag{4b}$$

However, P and T are both tracked as we move through the star. Therefore, these equations are rearranged as

$$P\left(\vec{X},\rho,T\right) \rightarrow \rho\left(\vec{X},P,T\right) \tag{5}$$

where we find the density ρ that yields the current value of P. Since the equations are non-linear, this is done via root finding, which is discussed in further detail in Section 3.1.

We also have equations for energy production via nuclear reaction chains [18]:

$$\epsilon\left(\vec{X},\rho,T\right) = \epsilon_{pp}\left(\vec{X},\rho,T\right) + \epsilon_{\text{CNO}}\left(\vec{X},\rho,T\right) + \epsilon_{3\alpha}\left(\vec{X},\rho,T\right) \tag{6}$$

$$\epsilon_{pp}\left(\vec{X},\rho,T\right) = 2.4\cdot 10^3\ \frac{\rho X_{\text{H}}^2}{T^{2/3}}\ \exp\left(-\frac{3.830\cdot 10^3}{T^{1/3}}\right) \tag{7a}$$

$$\epsilon_{\text{CNO}}\left(\vec{X},\rho,T\right) = 4.4\cdot 10^{24}\ \frac{\rho X_{\text{H}}\left(X_{\text{C}}+X_{\text{N}}+X_{\text{O}}\right)}{T^{2/3}}\ \exp\left(-\frac{15.288\cdot 10^3}{T^{1/3}}\right) \tag{7b}$$

$$\epsilon_{3\alpha}\left(\vec{X},\rho,T\right) = 5.1\cdot 10^{28}\ \frac{\rho^2 X_{\mathrm{He}}^3}{T^3}\ \exp\left(-\frac{4.4027\cdot 10^9}{T}\right) \tag{7c}$$

where ϵ_{pp} and ϵ_{CNO} represent hydrogen fusion via the *pp*-chain and CNO cycle, respectively; and $\epsilon_{3\alpha}$ represents helium fusion via the triple-α process. Since these reaction rates are exponentially suppressed with temperature, we do not need to turn them on and off manually.

The last major structure equations are for the opacity κ, which describe the cross-sectional area per unit mass. There are two opacity channels [18, 19]:

- Radiative
  - Electron scattering
  - Free-free absorption
  - Bound-free absorption
  - H^- absorption
- Conductive
  - Electron conduction
  - Photon conduction

$$\kappa_{\mathrm{rad}}\left(\vec{X},\rho,T\right) = \kappa_{e,\mathrm{rad}}\left(\vec{X}\right) + \kappa_{\text{f-f}}\left(\vec{X},\rho,T\right) + \kappa_{\text{b-f}}\left(\vec{X},\rho,T\right) + \kappa_{\mathrm{H^-}}\left(\vec{X},\rho,T\right) \tag{8a}$$

$$\kappa_{\mathrm{cond}}\left(\vec{X},\rho,T\right) = \kappa_{e,\mathrm{cond}}\left(\vec{X},\rho,T\right) + \kappa_{\gamma}\left(\vec{X},\rho,T\right) \tag{8b}$$

$$\kappa_{e,\mathrm{rad}}\left(\vec{X}\right) = 0.02\,(1+X_{\mathrm{H}}) \tag{9a}$$

$$\kappa_{\text{f-f}}\left(\vec{X},\rho,T\right) = 3.68\cdot 10^{22}\ \frac{X_{\mathrm{metals}}^2}{\mu_{\mathrm{ions}}\left(\vec{X}\right) m_e}\rho T^{-7/2} \tag{9b}$$

$$\kappa_{\text{b-f}}\left(\vec{X},\rho,T\right) = 4.34\cdot 10^{25}\ g\left(\vec{X},\rho\right)\ X_{\mathrm{metals}}\,(1+X_{\mathrm{H}})\,\rho T^{-7/2} \tag{9c}$$

$$\kappa_{\mathrm{H^-}} = 2.5\cdot 10^{-32}\ \frac{X_{\mathrm{metals}}}{0.02}\rho^{1/2}T^9\ \mathrm{sigmoid}(T,-2,5000) \tag{9d}$$

with the definition of the metals mass fraction

$$X_{\mathrm{metals}} = 1 - X_{\mathrm{H}} - X_{\mathrm{He}} \tag{10}$$

and the bound-free absorption guillotine factor [20, 21]

$$g\left(\vec{X},\rho\right) = \frac{1}{2.82\left(\rho\left(1+X_{\mathrm{H}}\right)\right)^2} \tag{11}$$

It is also worth noting that the H^- is suppressed at high temperatures using a sigmoid function, discussed in further detail in Section 3.1. This accounts for the increasing ionization fraction at high temperatures, which reduces the presence of H^-.

$$\kappa_{e,\mathrm{cond}}\left(\vec{X},\rho,T\right) = \frac{32\pi\sigma_{SB}T^3}{3k_B\rho}\left(\frac{m_e}{3k_BT}\right)^{1/2}\left(\frac{\bar{\mathcal{Z}}\left(\vec{X}\right)e^2}{4\pi\varepsilon_0 k_BT}\right)^2 \tag{12a}$$

$$\kappa_{\gamma}\left(\vec{X},\rho,T\right) = \kappa_{e,\mathrm{cond}}\left(\vec{X},\rho,T\right)\ \sqrt{3}\ \bar{\mathcal{Z}}\left(\vec{X}\right)\frac{P_{\mathrm{rad}}\left(\vec{X},\rho,T\right)}{P_e\left(\vec{X},\rho,T\right)}\left(\frac{m_ec^2}{k_BT}\right)^{5/2} \tag{12b}$$

with the definition of the average atomic number

$$\bar{\mathcal{Z}}\left(\vec{X}\right) = \sum_i X_i\mathcal{Z}_i \tag{13}$$

Note that the opacity sources within a channel add linearly, but the opacities from different channels add *harmonically*, yielding

$$\frac{1}{\kappa\left(\vec{X},\rho,T\right)} = \frac{1}{\kappa_{\mathrm{rad}}\left(\vec{X},\rho,T\right)} + \frac{1}{\kappa_{\mathrm{cond}}\left(\vec{X},\rho,T\right)} \tag{14}$$

2.3 Equations of Stellar Structure

With the equations of state in place, we can now define the equations of stellar structure that describe how our main variables $(r(m), P(m), L(m), T(m))$ change throughout the star with the mass coordinate m.

$$\frac{\partial r(m)}{\partial m} = \frac{1}{4\pi\ r^2(m)\ \rho\left(\vec{X},P(m),T(m)\right)} \tag{15a}$$

$$\frac{\partial P(m)}{\partial m} = -\frac{Gm}{4\pi\ r^4(m)} \tag{15b}$$

$$\frac{\partial L(m)}{\partial m} = \epsilon\left(\vec{X},\rho(m),T(m)\right) \tag{15c}$$

$$\frac{\partial T(m)}{\partial m} = \begin{cases} -\frac{3\ \kappa(m)\ L(m)}{256\pi^2\sigma_{SB}\ r^4(m)\ T^3(m)} & \text{radiative/conductive} \\ \left(1-\frac{1}{\gamma}\right)\frac{T(m)}{P(m)}\frac{\partial P(m)}{\partial m} & \text{convective} \end{cases} \tag{15d}$$

Note that Equation (15d) is a piecewise function that depends on the dominant energy transport mechanism [22]. This is given by the conditional [4]

$$\frac{P(m)}{T(m)}\left(\frac{\partial P(m)}{\partial T(m)}\right)^{-1} = \frac{\partial \ln T(m)}{\partial \ln P(m)} < \left(1-\frac{1}{\gamma}\right) \tag{16}$$

If this condition is true, then the dominant energy transport mechanism is radiation or conduction; otherwise, the dominant mechanism is convection.

2.4 Boundary Conditions

We also need to specify boundary conditions for our model. First, we have boundary conditions at the surface, where those for r and L are approximated from main sequence scaling relations [23, 24], and those for P and T are calculated analytically [24].

$$m = M \tag{17a}$$

$$L_{\text{surface}} = L(M) = \left(\frac{M}{M_\odot}\right)^{3.5} L_\odot + \delta L \tag{17b}$$

$$R = r(M) = \begin{cases} \left(\frac{M}{M_\odot}\right)^{0.8} R_\odot + \delta r & M \leq M_\odot \\ \left(\frac{M}{M_\odot}\right)^{0.57} R_\odot + \delta r & M > M_\odot \end{cases} \tag{17c}$$

$$T_{\text{surface}} = T(M) = \left(\frac{L_{\text{surface}}}{4\pi\sigma_{SB}\ R^2}\right)^{1/4} \tag{17d}$$

$$\begin{aligned} \rho_{\text{surface}} = \rho(M) = \sqrt{\frac{2}{3}}\Bigg[& 3.68\cdot 10^{22}\ \frac{X_{\text{metals}}^2}{\mu_{\text{ions}}\left(\vec{X}\right)\mu_e\left(\vec{X}\right)} T_{\text{surface}}^{-7/2} \\ & +4.24\cdot 10^{25}\ X_{\text{metals}}\left(1-X_{\text{H}}\right) T_{\text{surface}}^{-7/2} \\ & +\left(2.5\cdot 10^{-32}\ \frac{X_{\text{metals}}}{0.02} T_{\text{surface}}^{9}\ \text{sigmoid}\left(T_{\text{surface}}, -2, 5000\right)\right)^2\Bigg]^{-1/2} \end{aligned} \tag{17e}$$

$$\begin{aligned} \kappa_{\text{surface}} = \kappa(M) = & \kappa_{\text{f-f}}\left(\vec{X}, \rho_{\text{surface}}, T_{\text{surface}}\right) \\ & + \kappa_{\text{b-f}}\left(\vec{X}, \rho_{\text{surface}}, T_{\text{surface}}\right) + \kappa_{\text{H}^-}\left(\vec{X}, \rho_{\text{surface}}, T_{\text{surface}}\right) \end{aligned} \tag{17f}$$

$$P_{\text{surface}} = P(M) = \frac{2}{3}\frac{GM}{\kappa_{\text{surface}} R^2} + \frac{2}{3c}\frac{L_{\text{surface}}}{4\pi R^2} \tag{17g}$$

where we use an expansion for ρ_{surface} with an optical depth of $\tau = \frac{2}{3}$ and neglect opacity from conduction and electron scattering.

Then, we have boundary conditions at the center, where those for P and T are semi-empirically approximated from main sequence scaling relations [24–26], and those for r and L are calculated analytically.

$$\lim_{m \to 0} m = M_0 \implies \frac{M_0}{M} = 10^{-10} \ll 1 \tag{18a}$$

$$\rho_{\text{central}} = \rho(M_0) = 115.0 \frac{3}{4\pi}\frac{M}{R^3} \tag{18b}$$

$$R_{\text{central}} = r(M_0) = \left(\frac{3}{4\pi}\frac{M_0}{\rho_{\text{central}}}\right)^{1/3} \tag{18c}$$

$$P_{\text{central}} = P(M_0) = 7.701 \frac{GM^2}{R^4} + \delta P \tag{18d}$$

$$T_{\text{central}} = T(M_0) = \frac{2}{3}\frac{G}{k_B}\frac{M m_u}{R} + \delta T \tag{18e}$$

$$L_{\text{central}} = L(M_0) = M_0 \, \epsilon\left(\vec{X}, \rho_{\text{central}}, T_{\text{central}}\right) \tag{18f}$$

where I assume some small core mass M_0 with constant density, temperature, pressure, and energy production within the core.

3 Simulations

3.1 Numerical Implementation

Here, I will describe how all of the physics above is implemented in code, which is stored in a GitHub repository.

Each of the equations of state and their respective sub-elements are defined as functions taking the appropriate inputs (e.g., `pressure_ions(X, rho, T)`, `opacity_free_free(X, rho, T)`, etc.). The reduced luminosity is stored as a dictionary with different keys for each channel (`r"$pp$-chain"`, `r"$\mathrm{CNO}$"`, and `r"3-$\alpha$"`, respectively). The raw strings allow for LaTeX formatting during plotting.

There are a few additional utility functions, including:

- `root_finder(f, x0, x1, epsilon)` that uses bisection root finding on a function `f` between `x0` and `x1` up to some error tolerance `epsilon`. This is used in finding the density $\rho\left(\vec{X}, P, T\right)$ (see Equation (5)).

- `clamp(val, low, high)` that clamps `val` between `low` and `high`. Mathematically, this can be expressed as

$$\text{clamp}(x, x_0, x_1) = \max(x_0, \min(x_1, x))$$

  This is used when calculating perturbations, discussed in further detail in Section 3.3.

- `sigmoid(x, A, mu)` that applies the sigmoid function

$$\text{sigmoid}(x, A, \mu) = \frac{1}{1 + e^{-A(x-\mu)}}$$

  This is used in the H^- opacity κ_{H^-} (see Equation (9d)). Note that $A > 0$ corresponds to exponential strengthening for $x > \mu$, and $A < 0$ corresponds to exponential suppression.

There is also an empty class `DataContainer` that is used to store the astrophysical constants (`consts`) and information about the star and its boundary conditions (`STAR`).

The four main variables (r, P, L, T) are tracked in arrays `z1` and `z2`, representing the inward and outward solutions, respectively. There are corresponding masses `m1` and `m2`. There is a wrapper function `EOS(z, STAR)` that returns the density ρ, reduced luminosity ϵ, and total opacity κ; and a function `stellar_derivatives(z, m, STAR)` that returns the derivatives $\frac{\partial \vec{z}}{\partial m}$.

3.2 Integration Methods

The primary integration method uses 4th-order Runge-Kutta integration [27], which integrates the ODEs $f(\vec{x}, y)$ with respect to some independent variable y with a stepsize δy:

$$\begin{aligned}
\vec{k}_1 &= f(\vec{x}, y) \\
\vec{k}_2 &= f\left(\vec{x} + \frac{\vec{k}_1}{2}, y + \frac{\delta y}{2}\right) \\
\vec{k}_3 &= f\left(\vec{x} + \frac{\vec{k}_2}{2}, y + \frac{\delta y}{2}\right) \\
\vec{k}_4 &= f\left(\vec{x} + \vec{k}_3, y + \delta y\right)
\end{aligned} \tag{19}$$

such that

$$\vec{x} \to \vec{x} + \frac{1}{6}\left(\vec{k}_1 + 2\vec{k}_2 + 2\vec{k}_3 + \vec{k}_4\right) \tag{20}$$

When implemented in code, I integrate `stellar_derivatives(zi, m)` with a stepsize `hi`. This stepsize is pre-computed at each integration step. For each variable, we can define some characteristic integration lengthscale (as in [25])

$$\vec{h}_i \sim \left|\frac{\vec{z}_i}{\frac{\partial \vec{z}_i}{\partial m}}\right| = \left|\frac{\partial \ln \vec{z}_i}{\partial m}\right|^{-1}$$

that describes the stepsize such that $\vec{z}_i$ changes by its current order of magnitude. My code adopts the formula

$$h_i = \min\left(\frac{m_i}{100}, \xi \vec{h}_i\right) \tag{21}$$

where ξ is some stepsize scaling parameter. This means that the stepsize is at most 10% of the smallest characteristic lengthscale, but no more than 1% of the mass contained within the current shell. Note that $h_1 > 0$ (increasing mass outwards) and $h_2 < 0$ (decreasing mass inwards).

Another note on the implementation of the RK4 integration function is that it will throw an error if any elements of $\vec{z}_i$ become negative; this can happen because the derivative equations are piecewise and non-linear. In this case, h_i is reduced by an order of magnitude and the integration is attempted again.

3.3 Perturbations and Shooting

Beginning from the boundary conditions specified in Section 2.4, I integrate the solutions $\vec{z}_1$ and $\vec{z}_2$ towards each other until they meet at some mass m_{mid}. However, it is unlikely that the solutions will match at this point, which is because we have guessed four of the eight boundary conditions. In this case, following from [24], we can define the residuals

$$\vec{\mathcal{R}} = \vec{z}_2(m_{\text{mid}}) - \vec{z}_1(m_{\text{mid}}) \tag{22}$$

and use a shooting algorithm to determine updates to the boundary conditions that yield a better-matching solution. If we let $\vec{\mathcal{B}} = [R, P_{\text{central}}, L_{\text{surface}}, T_{\text{central}}]$ (the vector of guessed boundary conditions), then we want to solve the matrix equation

$$\sum_j \frac{\partial \mathcal{R}_i}{\partial \mathcal{B}_j} \delta \mathcal{B}_j = -\mathcal{R}_i \tag{23}$$

for the $\delta\mathcal{B}_j$'s, which are the updates to the boundary conditions in Equations (17) and (18). Each of the derivatives $\frac{\partial\vec{\mathcal{R}}}{\partial\mathcal{B}_j}$ requires an integration pass, meaning that each "perturbations pass" requires five integration passes (one unperturbed, and one with each of the four guessed boundary conditions perturbed). The perturbations are calculated as $\partial\vec{\mathcal{B}} = 1.01\vec{B}$.

In an attempt to preserve behavior of the solution, these updates are clamped to be within 10% of the original boundary condition; that is,

$$\frac{\delta\mathcal{B}_i}{\mathcal{B}_i} = \text{clamp}\left(\frac{\delta\mathcal{B}_i}{\mathcal{B}_i}, -0.1, 0.1\right) \tag{24}$$

3.4 Numerical Algorithm

With all of these different components, it would be useful to make clear the numerical algorithm that this program uses. It can be described as follows:

Full program

1. Specify total mass M and chemical composition $\vec{X}$

Perturbations pass

Integration pass

2. Specify external ($m = M$) and internal ($m = M_0 \ll M$) boundary conditions
3. Initialize variable arrays $\vec{z}_1$ (outward) and $\vec{z}_2$ (inward)

Integration step

4. Calculate intermediate variables (e.g., ρ, ϵ, κ) using equations of state
5. Calculate derivatives $\frac{\partial \vec{z}_i}{\partial m}$
6. Set stepsizes $h_i \sim \left|\frac{\partial \ln \vec{z}_i}{\partial m}\right|^{-1}$, with $h_1 > 0$ and $h_2 < 0$
7. Update solutions using 4^{th}-order Runge-Kutta integration

8. Take integration steps until $m_1 = m_2 = m_{\text{mid}}$
9. Calculate residuals $\vec{\mathcal{R}} = \vec{z}_2(m_{\text{mid}}) - \vec{z}_1(m_{\text{mid}})$

10. Perturb each guessed boundary condition and calculate new residuals (each requires a separate integration pass)
11. Calculate updates to boundary conditions ($\delta\vec{\mathcal{B}}$) by solving matrix equation $\sum_j \frac{\partial \mathcal{R}_i}{\partial \mathcal{B}_j} \delta\mathcal{B}_j = -\mathcal{R}_i$

12. Perform perturbations passes until fractional residuals are below some desired error tolerance ($\frac{\mathcal{R}_i}{\mathcal{B}_i} < \delta$)

4 Results

The results shown here are for the test case of the ZAMS Sun, assuming a total mass of $M = M_\odot$ and a solar chemical composition detailed in Table 4.

Results from the initial integration pass ("Pass 0") are shown in Figure 2. The model shows clear discontinuities between the inner and outer solutions at the midpoint, which is expected. All variables except mass and luminosity appear to be overextended (that is, the outward solution is larger than the inward solution when it should be smaller, and vice versa). Many of these display "hooks" as the outward solution overextends as it approaches the midpoint. The limiting variable for the stepsize for the outward solution appears to be mass or luminosity (both increase approximately exponentially); the limiting variable for the stepsize for the inward solution appears to be temperature or pressure very near the surface, then radius further into the star.

My model correctly predicts the general behaviors of the variables (m, r, L, κ increase outward and P, T, ρ, ϵ increase inward). Additionally, it recovers that energy production is dominated by hydrogen fusion via the *pp*-chain at all points in the star. It also seems to recover a transition point in the inward solution near the surface, which is likely where the temperature gradient switches from being convective to radiative as one moves towards the center.

Following this model, the program succeeded in making 6 perturbations passes before being killed. This took approximately two hours on my laptop, for approximately 4 minutes per integration pass. This varied depending on what other processes were running on my machine, with determined how much CPU power/memory were used for running the program.

Results following 6 perturbation passes are shown in Figure 3. The results appear to be nearly identical to the "Pass 0" results, which is due to two reasons:

1. Since all of these variables are changing by several orders of magnitude, they have been plotted on log-scale plots (and, in the case of ϵ, which varies by hundreds of orders of magnitude, $\log(\epsilon)$ is plotted on a log-scale). On these scales, it is difficult to discern differences of $\lesssim 10\%$.

2. The boundary conditions are very similar, but not identical.

Interestingly, the boundary conditions roughly oscillated between the initial conditions and those from the first perturbation pass ($\vec{\mathcal{B}}_0$ and $\vec{\mathcal{B}}_1$, respectively). I suspect what was happening here is that all the boundary conditions were clamped. In this case, the boundary conditions at later passes were not identical since the fractional updates depend on the boundary conditions. However, that fact that the conditions oscillated seems to suggest that

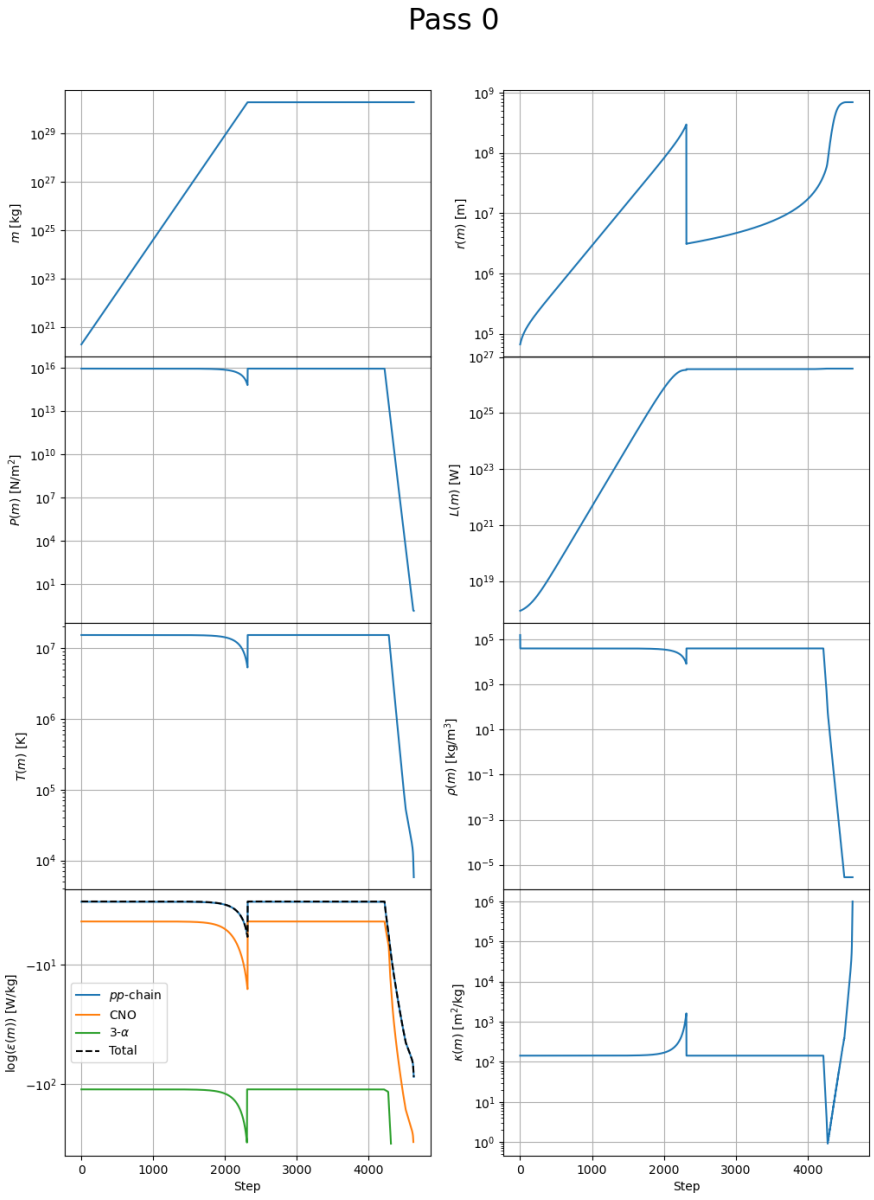

Figure 2: Model results for the Sun from initial (unperturbed) boundary conditions.

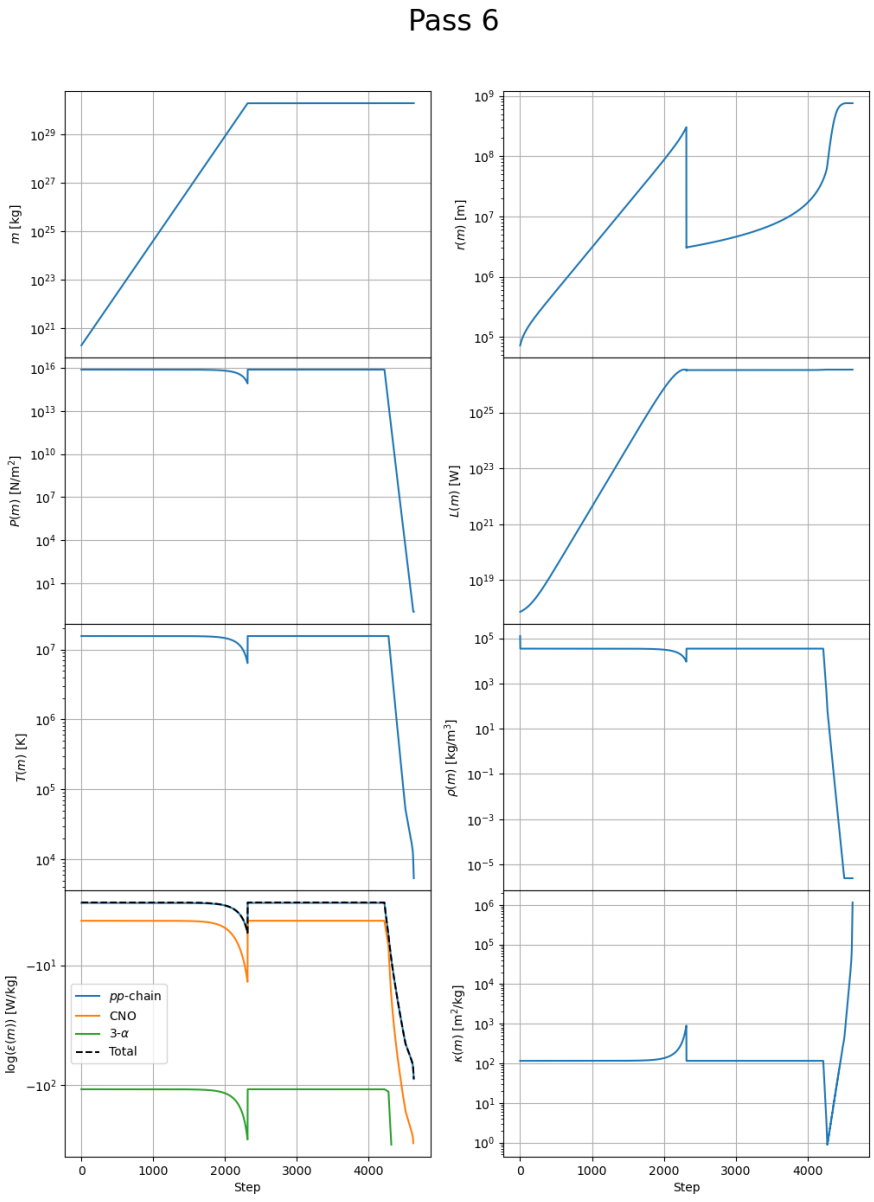

Figure 3: Model results for the Sun after 6 perturbation passes.

the ideal conditions lie somewhere between $\vec{\mathcal{B}}_0$ and $\vec{\mathcal{B}}_1$, which would preclude the need for clamping. Therefore, I am unable to explain this behavior.

5 Conclusions and Discussion

I have successfully created a program that can integrate the equations of stellar structure and attempts to improve the smoothness of the solutions using a shooting algorithm that updates the boundary conditions, and have tested its performance on the ZAMS Sun. This program was unable to converge to a smooth solution in the amount of time available for this project. However, there are a few key features that this model gets correct:

- Correct behavioral trends for primary and intermediate variables
  - m, r, L, κ increase outwards
  - P, T, ρ, ϵ increase inwards
- Energy production is dominated by the *pp*-chain at all points in the Sun
- A transition point in the outer layers of the Sun where energy transport shifts from convective near the surface to radiative deeper in the envelope

There are a variety of ways in which this work could be improved further:

- Running the program for more passes may improve convergence
- Running on a dedicated CPU to improve performance by decreasing runtime
  - Running on a supercomputer may help with this, and could allow for parallelization opportunities since the inward and outward solutions are largely independent of each other
- Running the program for additional stellar masses and chemical compositions
  - One of the initial goals of this project was to generate solutions for a variety of ZAMS stars to see if it can correctly reproduce the main sequence
  - This can also be used to see if it correctly predicts observed trends with varying metallicities or chemical compositions
- Extending the program to additional kinds of stars (namely, giant stars and white dwarfs, which are discussed in further detail below)

For extending to giants and white dwarfs, there are additional changes/complications that would need be addressed. I propose some potential solutions here:

- Giant stars:
  - Giant stars would require a different set of boundary conditions since they follow different scaling relations. For stars in the horizontal branch, their luminosities depend little on mass ($L \sim \mathcal{O}(50\ L_\odot)$) [28, 29]; rather, they depend on the relative masses of the helium core and hydrogen envelope.
  - The main complication for giant stars is that the assumption of an isotropic chemical composition is no longer valid. Instead, I propose having an array of mass fractions $\overleftrightarrow{X} = \left[\vec{X}_1, \vec{X}_2, \dots\right]$, where the mass fraction at each point is the one that yields the highest energy production. For the horizontal branch, there would be a transition point between the helium-enriched core and the surrounding hydrogen envelope.
  - Some giant stars reach high-order stages of burning, and several nuclear reaction chains would need to be considered for energy production. This can be implemented in tandem with $\overleftrightarrow{X}$.
- White dwarfs:
  - As with giants, white dwarfs would also need a distinct set of boundary conditions that reflect their scaling relations. There is no simple relationship between mass and luminosity that I was able to find. However, the white dwarf mass-radius scaling relation in well-known (e.g., [30, 31]):

$$R \approx 0.003 \left(\frac{M}{M_\odot}\right)^{-1/3} R_\odot \tag{25}$$

  - White dwarfs have different internal structures since they are incredibly dense. This manifests in electron degeneracy pressure and heat conduction being the dominant energy transport mechanism, though the program should already account for these.
  - The largest difference is that the white dwarf does not generate energy via nuclear fusion, so ϵ is not well-defined for white dwarfs. Instead, we expect the luminosity to depend only on the mass inside the current shell and its temperature. Therefore, if we defined some constant C as some temperature-dependent reduced luminosity, then the luminosity becomes [24]

$$L_{\rm WD}(m) = CmT_{\rm central} \implies \frac{\partial L_{\rm WD}(m)}{\partial m} = CT_{\rm central} \tag{26}$$

with $C \sim 2.59 \cdot 10^{-26}$ W/kg K.

References

[1] H. Kragh. "The Source of Solar Energy, ca. 1840-1910: From Meteoric Hypothesis to Radioactive Speculations". In: *EPJ H* 41.4-5 (Sept. 9, 2016). DOI: 10.1140/epjh/e2016-70045-7. URL: https://arxiv.org/abs/1609.02834.

[2] H. A. Bethe. "Energy Production in Stars". In: *Phys. Rev.* 55 (5 Mar. 1939), pp. 434–456. DOI: 10.1103/PhysRev.55.434. URL: https://link.aps.org/doi/10.1103/PhysRev.55.434.

[3] The Nobel Prize Organisation. *The Nobel Prize in Physics 1967*. 2023. URL: https://www.nobelprize.org/prizes/physics/1967/summary/.

[4] D. Prialnik. *An Introduction to the Theory of Stellar Structure and Evolution*. 2nd ed. Cambridge University Press, 2010. ISBN: 978-0-521-86604-0.

[5] B. Paxton et al. "Modules for Experiments in Stellar Astrophysics (MESA)". In: *The Astrophysical Journal Supplement Series* 192.1 (Dec. 2010), p. 3. DOI: 10.1088/0067-0049/192/1/3. URL: https://arxiv.org/abs/1009.1622.

[6] Wikipedia. *Planck's law*. Mar. 2023. URL: https://en.wikipedia.org/wiki/Planck%27s_law.

[7] E. Hertzsprung. "Über die Sterne der Unterabteilungen *c* und *ac* nach der Spektralklassifikation von Antonia C. Maury". In: *Astronomische Nachrichten* 179.24 (Jan. 1909), p. 373. DOI: 10.1002/asna.19081792402.

[8] H. Rosenberg. "Über den Zusammenhang von Helligkeit und Spektraltypus in den Plejaden". In: *Astronomische Nachrichten* 186.5 (Oct. 1910), p. 71. DOI: 10.1002/asna.19101860503.

[9] H. Russell. "Relations Between the Spectra and Other Characteristics of the Stars". In: *Popular Astronomy* 22 (May 1914), pp. 275–294.

[10] A. J. Cannon and E. C. Pickering. "The Henry Draper catalogue 0h, 1h, 2h, and 3h". In: *Annals of Harvard College Observatory* 91 (Jan. 1918), pp. 1–290.

[11] Wikipedia. *Annie Jump Cannon*. Jan. 2023. URL: https://en.wikipedia.org/wiki/Annie_Jump_Cannon.

[12] European Space Agency. *Hipparcos homepage*. URL: https://www.cosmos.esa.int/web/hipparcos.

[13] F. van Leeuwen. "The HIPPARCOS Mission". In: *Space Science Reviews* 81 (Aug. 1997), pp. 201–409. DOI: 10.1023/A:1005081918325.

[14] M.A.C. Perryman. "Hipparcos: Revised mission overview". In: *Advances in Space Research* 11 (2 1991). DOI: https://doi.org/10.1016/0273-1177(91)90464-U. URL: https://www.sciencedirect.com/science/article/pii/027311779190464U.

[15] European Space Agency. *Gaia homepage*. URL: https://www.cosmos.esa.int/web/gaia.

[16] F. van Leeuwen et al (*Gaia* Collaboration). *Gaia DR3 documentation*. Gaia DR3 documentation, European Space Agency; Gaia Data Processing and Analysis Consortium. Online at https://gea.esac.esa.int/archive/documentation/GDR3/index.html. June 2022.

[17] C. Babusiaux et al (*Gaia* Collaboration). "*Gaia* Data Release 2: Observational Hertzsprung-Russel Diagrams". In: *A&A* 616 (Aug. 2018), A10. DOI: 10.1051/0004-6361/201832843. URL: https://arxiv.org/abs/1804.09378.

[18] C. Hansen, S. Kawaler, and V. Trimble. *Stellar Interiors: Physical Principles, Structure, and Evolution*. 2nd ed. Springer, 2004. ISBN: 978-1-4612-6497-2. DOI: 10.1007/978-1-4419-9110-2.

[19] K. Wood. Lecture slides for AS 3003 at the University of St. Andrews. URL: http://www-star.st-and.ac.uk/~kw25/teaching/stars/STRUC7.pdf.

[20] B. Carroll and C. Ostile. *An Introduction to Modern Astrophysics*. 2nd ed. Cambridge University Press, 2017. ISBN: 978-1-108-42216-1. DOI: 10.1017/9781108380980.

[21] M. Richmond. Lecture notes for PHYS 370 at Rochester Institute of Technology. URL: http://spiff.rit.edu/classes/phys370/lectures/.

[22] Wikipedia. *Stellar structure*. Jan. 2023. URL: https://en.wikipedia.org/wiki/Stellar_structure.

[23] Wikipedia. *Mass-luminosity relation*. Apr. 2022. URL: https://en.wikipedia.org/wiki/Mass%E2%80%93luminosity_relation.

[24] R. Ciardullo. Lecture notes for A534 at Pennsylvania State University. URL: http://personal.psu.edu/rbc3/A534/.

[25] E. Brown. GitHub code for stellar integration for AST 304 at Michigan State University. Dec. 2020. URL: https://github.com/MSU-AST304-FS2020/Project3-main-sequence.

[26] Wikipedia. *Solar core*. Apr. 2023. URL: https://en.wikipedia.org/wiki/Solar_core.

[27] Wikipedia. *Runge-Kutta methods*. Apr. 2023. URL: https://en.wikipedia.org/wiki/Runge%E2%80%93Kutta_methods.

[28] J. Jackiewicz. Lecture notes for ASTR 565 at New Mexico State University. Apr. 2022. URL: http://astronomy.nmsu.edu/jasonj/565/.

[29] Wikipedia. *Horizontal branch*. Feb. 2023. URL: https://en.wikipedia.org/wiki/Horizontal_branch.

[30] C. Mihos. Lecture notes from ASTR 221 at Case Western Reserve University. 2005. URL: http://burro.case.edu/Academics/Astr221/.

[31] Wikipedia. *White dwarf*. May 2023. URL: https://en.wikipedia.org/wiki/White_dwarf.

[32] Wikipedia. *Sun*. Apr. 2023. URL: https://en.wikipedia.org/wiki/Sun.

A Additional Tables

Symbol	Meaning	Value with Units (SI)
$\mathcal{A}_i$	Species average atomic mass	See Table 3
$\mathcal{Z}_i$	Species atomic number	See Table 3
m_u	Nucleon mass	$1.660538782 \cdot 10^{-27}$ kg
k_B	Boltzmann constant	$1.3806504 \cdot 10^{-23}$ J/K
h	Planck's constant	$6.6260896 \cdot 10^{-34}$ J s
m_e	Electron mass	$9.10938215 \cdot 10^{-31}$ kg
c	Speed of light	$2.99792458 \cdot 10^{8}$ m/s
σ_{SB}	Stefan-Boltzmann constant	$5.6704 \cdot 10^{-8}$ W/m^2 K^4
e	Electron charge	$1.602176487 \cdot 10^{-19}$ C
ε_0	Electric permittivity of free space	$8.854187817 \cdot 10^{-12}$ s^4 A^2/kg m^3
G	Gravitational constant	$6.673 \cdot 10^{-11}$ m^3/kg s^2
γ	Adiabatic index	$\begin{cases} \frac{5}{3} & \text{non-relativistic} \\ \frac{4}{3} & \text{relativistic} \end{cases}$
$M_\odot$	Solar mass	$1.9891 \cdot 10^{30}$ kg
$R_\odot$	Solar radius	$6.95508 \cdot 10^{8}$ m
$L_\odot$	Solar luminosity	$3.84 \cdot 10^{26}$ W

Table 2: Astrophysical constants used in project.

Species	Atomic Number $\mathcal{Z}_i$	Atomic Mass $\mathcal{A}_i$
H	1	1.008
He	2	4.0026
Li	3	6.94
Be	4	9.1022
B	5	10.81
C	6	12.011
N	7	14.007
O	8	15.999
F	9	18.998
Ne	10	20.180
Na	11	22.990
Mg	12	24.305
Al	13	26.982
Si	14	28.085
P	15	30.974
S	16	32.06
Cl	17	35.45
Ar	18	39.948
K	19	39.098
Ca	20	40.078
Sc	21	44.956
Ti	22	47.867
V	23	50.942
Cr	24	51.996
Mn	25	54.938
Fe	26	55.845
Z	7.75	15.5

Table 3: Table of atomic numbers and masses for different species used in project. Species Z is used as a placeholder for any mass fractions that are not specified, where $\mathcal{A}_\mathrm{Z}$ represents an average of the solar metal composition and $\mathcal{Z}_\mathrm{Z} \approx \frac{\mathcal{A}_\mathrm{Z}}{2}$ follows the relationship for nuclear structure for low $\mathcal{Z}_i$.

Species	Mass fraction X_i
H	0.7346
He	0.2485
C	0.0029
N	0.0009
O	0.0077
Ne	0.0012
Mg	0.0005
Si	0.0007
S	0.0004
Fe	0.0016
Z	0.0001

Table 4: Solar chemical composition used in results [32]. See Table 3 for definition of species Z.